IEEE Access
Multidisciplinary | Rapid Review | Open Access Journal

Received 2 September 2022, accepted 21 September 2022, date of publication 30 September 2022, date of current version 7 October 2022.

Digital Object Identifier 10.1109/ACCESS.2022.3210938

RESEARCH ARTICLE

Closed-Form Bit Error Probability of ZF Detection for OFDM-M-MIMO Systems Using Effective Noise PDF

DITSAPON CHUMCHEWKUL[1] AND CHARALAMPOS C. TSIMENIDIS[2], (Senior Member, IEEE)
[1]School of Engineering, Newcastle University, NE1 7RU Newcastle upon Tyne, U.K.
[2]Department of Engineering, Nottingham Trent University, NG1 4FQ Nottingham, U.K.

Corresponding author: Ditsapon Chumchewkul (d.chumchewkul2@ncl.ac.uk)

This work was supported in part by the National Science and Technology Development Agency (NSTDA) under Grant ST G5671, and in part by the Engineering and Physical Sciences Research Council (EPSRC) under Grant EP/R002665/1.

ABSTRACT This paper derives the closed-form bit error probability (BEP) of massive multiple-input, multiple-output (M-MIMO) systems using orthogonal frequency-division multiplexing (OFDM) and zero-forcing (ZF) detection. We improve the BEP accuracy by increasing the Neumann series expansion (NSE) to second order for the system that we previously analyzed by deriving the probability distribution function (PDF) of the effective noise. The proposed PDF is then utilized to evaluate the BEP, the PDF of output signal-to-noise ratio (SNR), and the outage probability as a function of the output SNR of the system. Furthermore, a simplified closed-form expression for the effective noise PDF, in terms of the Gaussian distribution, and the noise variance are firstly derived in this paper for simplifying the performance analysis. Monte-Carlo simulation results confirm that the outcome from the derived equation and the approximation closely matched those obtained by simulation. In addition, we employ the proposed noise variance to estimate the log-likelihood ratio (LLR) instead of the approximate noise variance for the low-complexity soft-output ZF detection. The computational complexity of the proposed detection is thus significantly reduced, whereas its bit error rate (BER) is lower than that of the classical detection. Focusing on a 10×200 Coded-OFDM-M-MIMO system, 97.81% of multiplications, required for producing the LLR from the estimated symbol, were minimized by utilizing the proposed detection. Therefore, the derived equations can be efficiently used for analyzing the performance of OFDM-M-MIMO systems, and reducing the computational complexity of the soft-output ZF detection.

INDEX TERMS Massive multiple-input, multiple-output (M-MIMO), Neumann series expansion (NSE), orthogonal frequency-division multiplexing (OFDM), zero forcing (ZF) detection.

I. INTRODUCTION

Massive multiple-input, multiple-output (M-MIMO) has become a promising technique to enhance the spectral and energy efficiencies for the 5^{th} generation (5G) cellular networks [1]. Both the mobile terminals (MT) and the base station (BS) of M-MIMO systems can use several antennas for data communication, and the spatial multiplexing technique is utilized for enhancing the data transmission rate. Since the MT sends their messages using multiple transmit antennas over the same time slots, the received signal at the BS includes the effects of both co-channel interference (CCI) and thermal noise. Therefore, a M-MIMO symbol detector is required at the receiver to estimate the transmitted symbols from the CCI and noise contaminated signal. Although several symbol detection techniques can be chosen for receiver, the number of transmit and receive antennas in M-MIMO system is very large, and the complexity of M-MIMO detector greatly increases according to the number of antennas. As a result, the computational complexity of M-MIMO detection becomes a critical factor for the implementation of M-MIMO systems in practice [2]. Focusing on an uplink M-MIMO

The associate editor coordinating the review of this manuscript and approving it for publication was Luca Barletta.

system, where the number of the receive antennas is chosen to be larger than that of the transmit antennas, the Gram matrix of the system tends to be a diagonal matrix. As a result, linear symbol detection provides an excellent result to enhance the spectral and energy efficiencies of the system [1]. Maximal-ratio combining (MRC) detection has become an attractive technique to detect transmitted information symbols in practical M-MIMO systems, since the detector requires only a matrix multiplication to produce an estimated symbol. However, for a medium-size M-MIMO system, the number of the receive antennas is not much larger than that of the transmit antennas and the outcome from the MRC detection still contains remaining effects of CCI, thus, degrading system performance. Therefore, zero-forcing (ZF) and minimum mean square error (MMSE) detection are still required for this case. These detectors use inverse matrix operation to recover the contaminated symbol at the receiver and the computational complexity of the detection significantly increases according to the number of antennas. Thus, Neumann series expansion (NSE), Gauss-Seidal iteration, and other approximations can be utilized to reduce the computational complexity at the receiver [3], [4], [5], [6], [7], [8], [9]. If the number of the receive antennas is much larger than that of the transmit antennas, the outcome from the approximation significantly matches that of the general detection [3].

ZF detection is a classical linear symbol detection, which uses Moore-Penrose inverse matrix operation to recover contaminated symbols at the receiver. Generally, the bit error probability (BEP) of the system utilizing ZF detection is higher than that of MMSE detection for low signal-to-noise ratio (SNR). However, the computational complexity of the detection is less than that of the MMSE detection since the SNR information is not required by the detector [10]. Furthermore, the difference in BEP of ZF and MMSE detection at a higher SNR region is marginal. Therefore, a number of research works focused on BEP performance for this type of detection. Exponential tight bounds on BEP of the data communications using multiple antennas and optimal combining were proposed for flat and frequency-selective Rayleigh fading in [11] and [12]. The numerical results confirm that user capacity can be significantly enhanced by increasing the number of the antennas. The BEP of the MIMO system using ZF detection was then analyzed under various fading channels in [13] and [14]. The authors employed the complex Wishart distribution and a derived probability distribution function (PDF) of SNR in [15] to approximate the PDF of the Gram matrix. A closed-form expression for the BEP was also proposed in the work. In [16], the BEP of the system over uncorrelated Rayleigh fading channel was approximated. The Gram matrix was assumed to be a diagonal matrix and the BEP was then derived employing the Gaussian approximation. The output SNR, BEP, outage probabilities, diversity-multiplexing gain trade-off, and SNR gain of the MIMO system using ZF and MMSE detection over uncorrelated flat Rayleigh fading were extensively investigated in [17]. The interference-to-noise ratio and the output SNR at high SNR region were approximated. The equation for the latter was then utilized to derive a tight approximation of the BEP, outage probabilities, diversity-multiplexing gain trade-off for the system. The authors also demonstrated a gap between the performance of MMSE and ZF detection, which cannot be decreased at a higher SNR region. The gap was then rewritten in terms of a Hermitian quadratic form in [18], and the authors employed the equation to derive the PDF of SNR, the symbol error rate and the outage probabilities of the M-MIMO system. A BEP analysis for the MIMO system over correlated Rician and Rayleigh fading was derived in [19]. The noncentral Wishart distributed matrix was utilized to approximate the distribution of the Gram matrix, and the authors proved that the PDF of the SNR can be approximated as an infinite linear summation of the Gamma distribution. Channel estimation is generally employed to the receiver to estimate the information, making a deviation between the actual and the estimated information. As a result, the effects of channel estimation errors in ZF detection and the BEP approximation were then investigated by a number of research works. In [20], the authors utilized Taylor expansion to approximate the pseudo-inverse of the channel matrix and employed Gaussian random variable to model the channel estimation errors. The SNR and the BEP for the system using M-PSK and M-QAM were then derived in the work. The authors also demonstrated that the PDF of the SNR exhibits the Chi-square distribution. The BEP analysis was then extended to the M-MIMO system and a lower SNR region in [21]. Improved SNR and BEP analysis for M-QAM were introduced in the work. The BEP for MRC, ZF, and MMSE detection in M-MIMO system using pilot symbols to estimate the channel state information was derived in [22]. The average SNR and the BEP were derived in the work.

According to the literature survey, the BEP analysis for the MIMO system using ZF detection and BPSK modulation over uncorrelated frequency-flat Rayleigh fading channel at high SNR region was previously proposed in [17]. The BEP for M-QAM and other type of modulation schemes was neglected in the paper, however, the readers can employ the PDF of the derive SNR to derive the BEP using the equations in [23], [24]. Although the outcome from the derived equation significantly matched the exact BEP, the distribution of the effective noise in the work was assumed to be the Gaussian distribution. Therefore, an accurate effective noise PDF of ZF detection is still required to derive the BEP of the system utilizing channel coding techniques [24]. Moreover, most research work involving low-complexity linear symbol detection in [3], [4], [5], [6], [7], [8] and [9] assumed that the effective noise after the detection exhibits the Gaussian distribution. Thus, the soft-output linear symbol detection used the Gaussian assumption to produce the log-likelihood ratio (LLR) from the estimated transmit symbol. However, as far as the research literature goes, there is no prior research work that derives a closed-form expression of the noise variance. As a result, the soft-output linear symbol detector requires

most of the arithmetic operations to evaluate the exact noise variance for producing the LLR.

In this paper, we introduces an accurate PDF of the effective noise of ZF detection for orthogonal frequency-division multiplexing-M-MIMO (OFDM-M-MIMO) system for Gray-coded BPSK, QPSK, and M-QAM modulation types. This work is motivated by a derived effective noise PDF for the system, proposed in [25]. The authors in the work used NSE to approximate the inverse matrix operation as a Taylor series, and the effective noise PDF was then derived from the joint probability of the involved random variables. The BEP of the system with Gray-encoded M-QAM was analyzed utilizing the derived PDF. In addition, the pairwise error probability of the system was then determined from the PDF and was used to evaluate the upper-bounds of coded systems. Although the BEP analysis in [25] provided accurate analytical results, only the 1^{st} order of Taylor's series was used by the research work, and the Gram matrix was assumed to be a diagonal matrix. As a result, there is still a small deviation between the analytical results and the exact BEP. More accurate analytical results could be theoretically achieved if a higher order of Taylor's series is chosen for the analysis. Therefore, in this paper, we employ the NSE with the 2^{nd} order Taylor series to analyze the effect of noise in ZF detection and its PDF. The PDF is additionally utilized to determine the BEP performance, the PDF of output SNR, and outage probability as a function of the output SNR of the OFDM-M-MIMO system.

Although the derived equation provides an accurate result, their computational complexity is still too high. Therefore, we firstly prove that the effective noise PDF of ZF detection tends to become a zero-mean, complex-valued Gaussian distribution, and a simplified closed-form expression of the noise variance is then derived. In practice, the analytical results from the approximate PDF are closely matching those from the exact equation if the number of the receive antennas is larger than 100, and the ratio of number of the receive antennas to that of the transmit antennas is larger than 10. As a result, the classical Gaussian distribution approximation can be also utilized to simplify the performance analysis of OFDM-M-MIMO system for special cases. Furthermore, we utilize the Gaussian approximation to reduce the computational complexity of the soft-output ZF detection. The proposed detector uses the derived noise variance for producing the LLR instead of the exact noise variance. Since the effective noise tends to become a Gaussian distribution, the BEP of the proposed detection is theoretically close to that of the classical detection, whereas its operational complexity can be significantly minimized.

The remainder of this article is organized as follows. A block diagram of the OFDM-M-MIMO system and the channel model are described in the next section. In section III, the operation of classical ZF detection is summarized. The effective noise of ZF detection and its PDFs are then analyzed in section IV. The Gaussian approximation of the effective noise of ZF detection is derived in section V. We also use these derived PDFs to analyze BEP performance, the PDF of the output SNR, and the outage probability of the OFDM-M-MIMO system utilizing ZF detection in sections VI to VIII, respectively. Furthermore, the operation of the proposed low-complexity soft-output ZF detection is summarized in the section IX, where the derived noise variance is used to produce the LLRs. We use Monte-Carlo simulations to demonstrate the validity of the proposed equations and obtain numerical results to evaluate the system performance, and the results are discussed in the section X.

Notation: In this paragraph, we clarify the notation of mathematical symbols used in this paper. We use bold characters $\mathbf{H}$ to denote matrix and vector variables. Their elements are written as $H_{n,m}$. Let $\lambda = I, Q$, the symbol $H^{\lambda}_{n,m}$ represents the in-phase and the quadrature component of $H_{n,m}$. The operator $(\,.)^{\dagger}$ denotes the Hermitian transpose of a matrix or vector and is equivalent to complex conjugate $(\,.)^{*}$ transposition $(\,.)^{T}$, e.g., $\mathbf{H}_f^{\dagger} = \left((\mathbf{H}_f)^T\right)^*$. $\Gamma(a)$ represents Gamma function of a, and the upper incomplete Gamma function is $\Gamma(a, b)$.

II. SYSTEM MODEL

Fig. 1 illustrates the block diagram of an uplink OFDM-M-MIMO system considered in this paper. The M-QAM mapper requires $N = N_b N_t N_f$ bits, where $N_b = \log 2(M)$. N_t represents the number of transmit antennas, and N_f is the number of sub-carriers in frequency domain. M denotes the QAM order and additionally corresponds to the number of points in the signal constellation. In practice, N_f is chosen to be a power of 2 so that the inverse fast-Fourier transform (IFFT) can be used to transfer the M-QAM symbols from frequency to time domain. The M-QAM mapper produces a symbol matrix, $\mathbf{X} \in \mathbb{C}^{N_t \times N_f}$, and the IFFT is applied row-wise to obtain a matrix $\Psi \in \mathbb{C}^{N_t \times N_f}$. Subsequently, N_{cp} cyclic prefix (CP) samples are appended to Ψ to eliminate the effect of inter-block interference (IBI) induced by the delay spread, τ, of the M-MIMO multipath channels. To avoid IBI, N_{cp} is chosen to be greater than τ. The resulting symbol is transmitted through the frequency-selective Rayleigh fading M-MIMO channel.

At the BS, the cyclic prefix samples are removed from the received signal and a fast-Fourier transform (FFT) is applied row-wise to transfer the signal in frequency domain and produce $\mathbf{Y} \in \mathbb{C}^{N_r \times N_f}$, where N_r is the number of receive antennas. This matrix is used by the M-MIMO detector to obtain the estimate, $\hat{\mathbf{X}}$, of the transmitted symbol matrix, $\mathbf{X}$. Finally, the receiver uses an M-QAM demapper to estimate the transmitted N information bits. By designing $N_{\text{cp}} > \tau$, the IBI is assumed to be completely eliminated. As a result, the received signal in frequency domain can be expressed as a linear matrix equation. Let $f = 0, 1, \ldots, N_f - 1$ denotes the sub-carrier index, and $\mathbf{X}_f \in \mathbb{C}^{N_t \times 1}$ be the vector of the transmit symbols of the f-th sub-carrier, with elements $\{X_m\}_{m=1}^{N_t}$. The value of X_m is chosen from a square-shaped M-QAM constellation, and the probability of the occurrence of each symbol is identical, i.e., $1/M$. The average transmit

energy per symbol is denoted as E_s. By assuming that the IBI is completely eliminated by utilizing a CP, the received symbol vector of the f-th sub-carrier $\mathbf{Y}_f \in \mathbb{C}^{N_r \times 1}$ can be expressed as

$$\mathbf{Y}_f = \mathbf{H}_f \mathbf{X}_f + \mathbf{W}_f, \tag{1}$$

where $\mathbf{H}_f \in \mathbb{C}^{N_r \times N_t}$ is channel frequency response (CFR) matrix of the f-th sub-carrier. If there is no line-of-sight link between transmitter and receiver, each component $H_{n,m}$ in $\mathbf{H}_f$ is represented by zero-mean, complex-valued, Gaussian random variables $\mathcal{CN}(0, 2\sigma_h^2)$ [26]. Their variance per dimension σ_h^2 is 0.5 so that the channel energy is normalized. Furthermore, $\mathbf{W}_f \in \mathbb{C}^{N_r \times 1}$ represents the vector of additive white Gaussian noise (AWGN). Each element, $\{W_n\}_{n=1}^{N_r}$, in $\mathbf{W}_f$ exhibits a zero-mean, complex-valued, Gaussian distribution, i.e., $\mathcal{CN}(0, 2\sigma_w^2)$, and σ_w^2 is determined by

$$\sigma_w^2 = \frac{N_t E_s}{2\log_2(M)\gamma_b}, \tag{2}$$

where γ_b is the signal-to-noise ratio (SNR) per bit. It is worth pointing out that data communication links using OFDM waveforms are generally degraded due to the carrier frequency offset (CFO) and channel estimation errors. As a result, more accurate mathematical expressions of the received symbol and the performance analysis were essentially proposed by a number of research work [27], [28], [29], [30]. However, considering CFO and other impairments such as IQ imbalance and frame synchronization in the system model is beyond the scope of this work. Utilizing all these impairments simultaneously to analyze the performance of the OFDM-M-MIMO system will become too complex. Therefore, the PDF of $H_{n,m}$ in (1) is assumed to be the Gaussian distribution for simplifying the performance analysis.

III. CLASSICAL ZF DETECTION

In this section, we discuss the operation of ZF detection and the effect of noise in its performance. The detection employs Moore-Penrose pseudoinverse of the CFR matrix to estimate the transmitted symbol from $\mathbf{Y}_f$ as [2]

$$\hat{\mathbf{X}}_f = (\mathbf{H}_f^\dagger \mathbf{H}_f)^{-1} \mathbf{H}_f^\dagger \mathbf{Y}_f. \tag{3}$$

Substituting $\mathbf{Y}_f$ from (1) in (3), we obtain

$$\hat{\mathbf{X}}_f = \mathbf{X}_f + \mathbf{G}_f^{-1} \mathbf{H}_f^\dagger \mathbf{W}_f, \tag{4}$$

where the Gram matrix is denoted as $\mathbf{G}_f = \mathbf{H}_f^\dagger \mathbf{H}_f \in \mathbb{C}^{N_t \times N_t}$. The receiver uses $\hat{\mathbf{X}}_f$ in (3) to determine the received message, and this symbol is usually contaminated by the effective noise $\mathbf{Z}_f = \mathbf{G}_f^{-1} \mathbf{H}_f^\dagger \mathbf{W}_f$. Let Z_m denotes the m-th vector element in $\mathbf{Z}_f \in \mathbb{C}^{N_t \times 1}$. In order to analyze the distribution of Z_m, the NSE approach is utilized to approximate the inverse matrix operation of the Gram matrix [3], i.e.,

$$\mathbf{G}_f^{-1} \simeq \sum_{l=0}^{L-1} (-\mathbf{D}_f^{-1} \mathbf{E}_f)^l \mathbf{D}_f^{-1}, \tag{5}$$

where the diagonal and off-diagonal components of $\mathbf{G}_f$ are represented as $\mathbf{D}_f$ and $\mathbf{E}_f$, respectively. Here, the elements of $\mathbf{D}_f$ and $\mathbf{E}_f$ are denoted as $D_{m,m} = \sum_{n=1}^{N_r} |H_{n,m}|^2$ and $E_{m,n} = \sum_{k=1}^{N_r} H_{k,m}^* H_{k,n}$, respectively. Generally, the order L of Taylor series in (5) should be large enough to minimize the differences between $\mathbf{G}_f^{-1}$ from (5) and their actual inverse matrix operation. However, since N_r in M-MIMO system is much larger than N_t, the results from NSE with $L = 2$ can provide an accurate result for this case. If $\mathbf{G}_f^{-1}$ in (5) and $L = 2$ are substituted in (4), $\mathbf{Z}_f$ becomes

$$\mathbf{Z}_f = (\mathbf{I} - \mathbf{D}_f^{-1} \mathbf{E}_f) \mathbf{D}_f^{-1} \mathbf{H}_f^\dagger \mathbf{W}_f. \tag{6}$$

Let $\mathbf{A}_f = \mathbf{H}_f^\dagger \mathbf{W}_f$, with elements $\alpha_m = \sum_{n=1}^{N_r} H_{n,m}^* W_n$, each component of $\mathbf{Z}_f$ in (6) can be written as

$$Z_m = \frac{1}{D_{m,m}} \left(\alpha_m - \sum_{n=1, n\neq m}^{N_t} \frac{E_{m,n}\alpha_n}{D_{n,n}} \right). \tag{7}$$

It is worth noting that a higher order L of Taylor series in (5) is not applied for this research work since the mathematical expression of Z_m for this case involves with dependent variables. As a result, the derived PDF, obtained by joint probabilities of the random variables, is still inaccurate.

IV. DERIVING EFFECTIVE NOISE PDF OF ZF DETECTION

Z_m, in (7), shows the effects of noise for the received symbol of ZF detection, and their distribution depends on N_t, N_r, and the operating SNR point of the OFDM-M-MIMO system. We now use this equation to derive the PDF of Z_m. Due to the fact that $D_{m,m}$, $E_{m,n}$, and α_m in (7) are functions of random variables, their joint probabilities can be used to derive their PDFs. However, there are several arithmetic operation in (7), and determining the PDF of Z_m is complex. Therefore, approximations are now utilized to simplify this operation. The PDF of $D_{m,m}$ was previously derived from (8) in [25]. Since $D_{m,m}$ can be rewritten as a $2N_r$ times summation of squared, zero-mean, Gaussian random variables with variance, σ_h^2, the PDF of $D_{m,m}$, $p_D(D_{m,m})$, exhibits a Chi-square distribution and tends to be the $\mathcal{N}(2N_r\sigma_h^2, 2N_r\sigma_h^2)$ if N_r is large enough [31]. Focusing on an OFDM-M-MIMO system where $N_r = 100$, the probability of the occurrence of $D_{m,m}$, ranging from 85 to 115, is 86.76%. Therefore, if $N_r \geq 100$, most of the variation of $D_{m,m}$ is less than 15% of its mean and $D_{m,m}$ can be approximated as a constant Δ, i.e.,

$$\Delta = 2N_r\sigma_h^2. \tag{8}$$

If Δ in (8) is substituted into (7), Z_m becomes

$$Z_m = \frac{\alpha_m}{\Delta} - \frac{1}{\Delta^2} \sum_{n=1, n\neq m}^{N_t} E_{m,n}\alpha_n. \tag{9}$$

Let $\tilde{\alpha}_m = \alpha_m/\Delta$, $\beta_m = \sum_{n=1, n\neq m}^{N_t} E_{m,n}\alpha_n$ and $\tilde{\beta}_m = \beta_m/\Delta^2$, (9) can be expressed as

$$Z_m = \tilde{\alpha}_m - \tilde{\beta}_m. \tag{10}$$

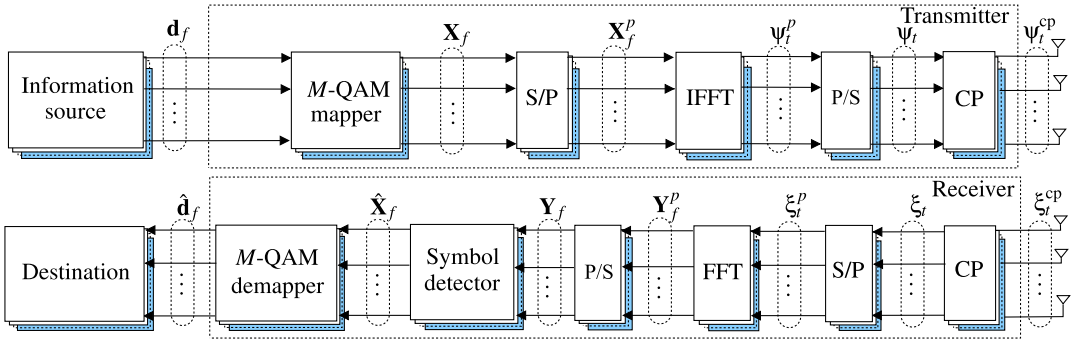

FIGURE 1. Block diagram of OFDM-M-MIMO system.

Undoubtedly, α_m, β_m, $\tilde{\alpha}_m$, $\tilde{\beta}_m$ and Z_m are a function of CFR and noise vector element W_n. Therefore, their PDFs can be derived utilizing joint probabilities as described in the next sub-sections.

A. THE APPROXIMATE PDF OF $E_{m,n}$

$E_{m,n}$ is an off-diagonal element of $\mathbf{G}_f$. The in-phase and quadrature components of $E_{m,n}$ can be expressed as

$$E^I_{m,n} = \sum_{k=1}^{N_r} H^{*,I}_{k,m} H^I_{k,n} - \sum_{k=1}^{N_r} H^{*,Q}_{k,m} H^Q_{k,n}, \tag{11a}$$

$$E^Q_{m,n} = \sum_{k=1}^{N_r} H^{*,I}_{k,m} H^Q_{k,n} + \sum_{k=1}^{N_r} H^{*,Q}_{k,m} H^I_{k,n}. \tag{11b}$$

Due to the fact that $H^{\lambda}_{n,m}$ is a Gaussian random variable with $\lambda = \{I, Q\}$, $E^{\lambda}_{m,n}$, in (11), is $2N_r$ times the summation of the product of two $\mathcal{N}(0, \sigma_h^2)$. For the system with large N_r, the PDF of $E^{\lambda}_{m,n}$ tends to become a Gaussian distribution $\mathcal{N}(0, \sigma_E^2)$, and the variance per dimension is given as

$$\sigma_E^2 = 2N_r \sigma_h^4. \tag{12}$$

B. DERIVING PDF OF α_m AND β_m

$\mathbf{A}_f$ is a product of $\mathbf{H}_f^{\dagger}$ and $\mathbf{W}_f$. Therefore, the in-phase and quadrature elements of α_m, in (7), can be expressed as

$$\alpha^I_m = \sum_{n=1}^{N_r} H^{*,I}_{n,m} W^I_n - \sum_{n=1}^{N_r} H^{*,Q}_{n,m} W^Q_n, \tag{13a}$$

$$\alpha^Q_m = \sum_{n=1}^{N_r} H^{*,I}_{n,m} W^Q_n + \sum_{n=1}^{N_r} H^{*,Q}_{n,m} W^I_n. \tag{13b}$$

Due to the fact that α^{λ}_m in (13) is $2N_r$ times the summation of the product of $H^{*,\lambda}_{n,m}$ and W^{λ}_n, their PDF is determined utilizing (6.9) of [32] and the results from this operation are

$$p_{\alpha}(\alpha^{\lambda}_m) = \frac{1}{\Gamma(N_r)} \exp\left(-\frac{|\alpha^{\lambda}_m|}{\sigma_h \sigma_w}\right) \times \sum_{k=1}^{N_r} \frac{(N_r + k - 2)! |\alpha^{\lambda}_m|^{N_r - k}}{2^{N_r + k - 1} (\sigma_h \sigma_w)^{N_r - k + 1} (N_r - k)! \Gamma(k)}. \tag{14}$$

In addition, if N_r is large enough, $p_{\alpha}(\alpha^{\lambda}_m)$ can be approximated as a $N(0, \sigma_{\alpha}^2)$, and their variance per dimension is given as

$$\sigma_{\alpha}^2 = 2\sigma_h^2 \sigma_w^2 N_r. \tag{15}$$

The PDF of β_m is also derived utilizing the joint probabilities of random variables. β^{λ}_m, in (9), is $2(N_t - 1)$ times the summation of the product of $E^{\lambda}_{m,n}$ and α^{λ}_m. If N_r is large enough, these variables tend to be a Gaussian distribution. Therefore, we can use (6.9) in [32] to determine the PDF of β^{λ}_m. As a result, $p_{\beta}(\beta^{\lambda}_m)$ becomes as (16), shown at the bottom of the page.

C. PDF OF $\tilde{\alpha}_m$ AND $\tilde{\beta}_m$

$\tilde{\alpha}_m$ and $\tilde{\beta}_m$ in (10) are ratio of α_m and β_m to constants, and their PDF can be obtained utilizing $p_{\alpha}(\alpha^{\lambda}_m)$, $p_{\beta}(\beta^{\lambda}_m)$, and (4.19) in [31], i.e.,

$$p_{\tilde{\alpha}}(\tilde{\alpha}^{\lambda}_m) = \Delta p_{\alpha}(\Delta \tilde{\alpha}^{\lambda}_m), \tag{17a}$$

$$p_{\tilde{\beta}}(\tilde{\beta}^{\lambda}_m) = \Delta^2 p_{\beta}(\Delta^2 \tilde{\beta}^{\lambda}_m). \tag{17b}$$

Substituting $p_{\alpha}(\alpha^{\lambda}_m)$, $p_{\beta}(\beta^{\lambda}_m)$, and Δ from (14), (16), and (8) into (17), the PDFs of $\tilde{\alpha}^{\lambda}_m$ and $\tilde{\beta}^{\lambda}_m$ become

$$p_{\tilde{\alpha}}(\tilde{\alpha}^{\lambda}_m) = \sum_{k=1}^{N_r} f_{\tilde{\alpha}}(k) |\tilde{\alpha}^{\lambda}_m|^{N_r - k} e^{\left(-\frac{2N_r \sigma_h |\tilde{\alpha}^{\lambda}_m|}{\sigma_w}\right)}, \tag{18a}$$

$$p_{\tilde{\beta}}(\tilde{\beta}^{\lambda}_m) = \sum_{k=1}^{N_t - 1} f_{\tilde{\beta}}(k) |\tilde{\beta}^{\lambda}_m|^{N_t - k - 1} e^{\left(-\frac{2N_r \sigma_h |\tilde{\beta}^{\lambda}_m|}{\sigma_w}\right)}. \tag{18b}$$

The function $f_{\tilde{\alpha}}(k)$ and $f_{\tilde{\beta}}(k)$ in (18) are defined as

$$f_{\tilde{\alpha}}(k) = \frac{(N_r \sigma_h)^{N_r - k + 1} (N_r + k - 2)!}{2^{2k-2} \sigma_w^{N_r - k + 1} \Gamma(N_r) \Gamma(k) (N_r - k)!}, \tag{19a}$$

$$p_{\beta}(\beta^{\lambda}_m) = \frac{1}{2^{2N_t - 2}} \exp\left(-\frac{|\beta^{\lambda}_m|}{2N_r \sigma_h^3 \sigma_w}\right) \sum_{k=1}^{N_t - 1} \frac{(N_t + k - 3)! |\beta^{\lambda}_m|^{N_t - k - 1}}{(N_r \sigma_h^3 \sigma_w)^{N_t - k} (N_t - 2)! (N_t - k - 1)! \Gamma(k)}. \tag{16}$$

$$f_{\tilde{\beta}}(k) = \frac{(N_r\sigma_h)^{N_t-k}(N_t+k-3)!}{2^{2k-2}\sigma_w^{N_t-k}\Gamma(k)(N_t-2)!(N_t-k-1)!}. \quad (19b)$$

D. EFFECTIVE NOISE PDF OF ZF DETECTION

According to (10), Z_m is a subtraction of $\tilde{\alpha}_m$ and $\tilde{\beta}_m$. Due to $p_{\tilde{\alpha}}(\tilde{\alpha}_m^\lambda)$ and $p_{\tilde{\beta}}(\tilde{\beta}_m^\lambda)$ are even functions, the PDF of Z_m^λ is analyzed by utilizing convolution integral operation [31], i.e.,

$$p_z(Z_m^\lambda) = p_{\tilde{\alpha}}(\tilde{\alpha}_m^\lambda) * p_{\tilde{\beta}}(\tilde{\beta}_m^\lambda). \quad (20)$$

If the PDFs of $\tilde{\alpha}_m^\lambda$ and $\tilde{\beta}_m^\lambda$ from (18) are substituted into (20) and the binomial expansion is employed to decompose the polynomial in the equation, the results from the integral operation becomes (21), as shown at the bottom of the page, i.e., the PDF of the effective noise of ZF detection. The function $f_z(k,p)$ in (21) is defined as

$$f_z(k,p) = \frac{(N_r+k-2)!(N_t+p-3)!}{2^{2k+2p-4}(N_t-2)!(N_r-k)!\Gamma(N_r)\Gamma(k)\Gamma(p)} \times \left(\frac{N_r\sigma_h}{\sigma_w}\right)^{N_t+N_r-k-p+1}. \quad (22)$$

V. THE GAUSSIAN APPROXIMATION OF $p_z(Z_m^\lambda)$

Although $p_z(Z_m^\lambda)$ in (21) provides an accurate noise PDF of ZF detection, their computation is complex and using this equation to determine performance of OFDM-M-MIMO system is still inconvenient. Therefore, we now prove that the PDF of Z_m^λ can be alternatively approximated as a classical Gaussian distribution. The variance of Z_m^λ is also analyzed in this section. If N_r is large enough, both α_m^λ and $E_{m,n}^\lambda$ can be approximated as a Gaussian random variable. If we use (17a) to derive the PDF of $\tilde{\alpha}_m^\lambda$, their distribution becomes Gaussian too, i.e., $\mathcal{N}(0,\sigma_{\tilde{\alpha}}^2)$, and the variance of this random variable can be expressed as σ_α^2/Δ^2, i.e.,

$$\sigma_{\tilde{\alpha}}^2 = \frac{\sigma_w^2}{2N_r\sigma_h^2}. \quad (23)$$

In addition, β_m^λ is $2(N_t-1)$ times the summation of the product of α_m^λ and $E_{m,n}^\lambda$. Therefore, it can be approximated as a $\mathcal{N}(0,2\sigma_\beta^2)$, and their variance σ_β^2 is $2(N_t-1)\sigma_E^2\sigma_\alpha^2$. By using (17b), $\tilde{\beta}_m^\lambda$ is also a Gaussian distribution. Its variance is determined by

$$\sigma_{\tilde{\beta}}^2 = \frac{2(N_t-1)\sigma_E^2\sigma_\alpha^2}{\Delta^4}. \quad (24)$$

Substituting σ_E^2 and σ_α^2 from (12) and (15) into (24), this equation becomes

$$\sigma_{\tilde{\beta}}^2 = \frac{(N_t-1)\sigma_w^2}{2N_r^2\sigma_h^2}. \quad (25)$$

Due to the fact that Z_m, in (10), is constructed by subtracting $\tilde{\alpha}_m$ from $\tilde{\beta}_m$, and both of them are approximated by a Gaussian distribution, the PDF of Z_m^λ becomes a $\mathcal{N}(0,\sigma_z^2)$ too, i.e.,

$$p_z(Z_m^\lambda) \simeq \frac{1}{\sqrt{2\pi\sigma_z^2}}\exp\left(-\frac{(Z_m^\lambda)^2}{2\sigma_z^2}\right). \quad (26)$$

σ_z^2 can be determined from sum of $\sigma_{\tilde{\alpha}}^2$ in (23) and $\sigma_{\tilde{\beta}}^2$ in (25), and the result from this operation is

$$\sigma_z^2 = \frac{\sigma_w^2}{\sigma_h^2}\left(\frac{1}{2N_r} + \frac{N_t-1}{2N_r^2}\right). \quad (27)$$

VI. BEP ANALYSIS

In the previous section, we have derived the effective noise PDF of ZF detection in (21) as well as their Gaussian approximation in (26). We now use these PDFs to evaluate the BEP performance of the proposed OFDM-M-MIMO system. If the transmitter uses BPSK, QPSK or squared-shape M-QAM modulation with Gray encoding, the receiver estimates the transmitted message from the in-phase and quadrature components of the received symbols independently. Let M_λ represent the number of constellation points per dimension, the symbol error probability (SEP) of the system is determined by averaging the error probabilities of $M_\lambda-2$ inner and 2 outer constellation points in each dimension. As a result, the SEP can be expressed as (5.105) in [26], i.e.,

$$P_s = \frac{2(M_\lambda-1)}{M_\lambda}P(\hat{X}_m^\lambda|X_m^\lambda = \bar{X}_m^\lambda, K). \quad (28)$$

$P(\hat{X}_m^\lambda|X_m^\lambda = \bar{X}_m^\lambda, K)$ in (28) denotes the cumulative distribution function (CDF) of Z_m^λ. The CDF demonstrates a pairwise error probability that a constellation point is transmitted by the transmitter and a nearest constellation point $\bar{X}_m^\lambda$ is detected by the receiver. The equation is written in terms of $p_z(Z_m^\lambda)$ as

$$P(\hat{X}_m^\lambda|X_m^\lambda = \bar{X}_m^\lambda, K) = \int_0^\infty p_z(Z_m^\lambda + K)dZ_m^\lambda, \quad (29)$$

where the shortest distance between the constellation points in each dimension and the decision boundary is denoted as

$$p_z(Z_m^\lambda) = e^{\left(-\frac{2N_r\sigma_h|Z_m^\lambda|}{\sigma_w}\right)}\sum_{k=1}^{N_r}\sum_{p=1}^{N_t-1}f_z(k,p)\sum_{q=0}^{N_t-p-1}\frac{1}{(N_t-p-q-1)!q!} \times\left(\frac{(-1)^q|Z_m^\lambda|^{N_t+N_r-k-p}}{N_r-k+q+1} + (N_t+N_r-k-p-q-1)!|Z_m^\lambda|^q\left(\frac{\sigma_w}{4N_r\sigma_h}\right)^{N_t+N_r-k-p-q} + \sum_{r=0}^{N_t+N_r-k-p-q-1}\frac{(-1)^q(N_t+N_r-k-p-q-1)!|Z_m^\lambda|^{N_t+N_r-k-p-r-1}}{(N_t+N_r-k-p-q-r-1)!}\left(\frac{\sigma_w}{4N_r\sigma_h}\right)^{r+1}\right). \quad (21)$$

K, i.e., 1 for 16-QAM using the constellation points per dimension $\{-3, -1, 1, 3\}$. We then utilize the P_s in (28) to derive the BEP as $P_s/\log_2(M_\lambda)$ [26], and results in

$$P_e = \frac{2(M_\lambda - 1)}{M_\lambda \log_2(M_\lambda)} P(\hat{X}_m^\lambda | X_m^\lambda = \bar{X}_m^\lambda, K). \tag{30}$$

By substituting the PDF of Z_m^λ from (21) in (29) and utilizing the binomial expansion to expand the polynomial, $P(\hat{X}_m^\lambda | X_m^\lambda = \bar{X}_m^\lambda, K)$ becomes (31), as shown at the bottom of the page. We use $P(\hat{X}_m^\lambda | X_m^\lambda = \bar{X}_m^\lambda, K)$ in the equation to evaluate the BEP of the proposed OFDM-M-MIMO system in (30). For example, if BPSK or QPSK modulation is selected, the constellation points per dimension, K, and M_λ are $\{-1, 1\}$, 1, and 2, respectively. By substituting these variables into (30), the BEP analysis for the system with BPSK and QPSK modulation becomes

$$P_e^{\text{BPSK,QPSK}} = P(\hat{X}_m^\lambda | X_m^\lambda = \bar{X}_m^\lambda, K = 1). \tag{32}$$

In addition, if the system utilizes 16-QAM modulation with the constellation points $\{-3, -1, 1, 3\}$, $K = 1$, and $M_\lambda = 4$. Therefore, the BEP in (30) is written as

$$P_e^{\text{16-QAM}} = \frac{3}{4} P(\hat{X}_m^\lambda | X_m^\lambda = \bar{X}_m^\lambda, K = 1). \tag{33}$$

It is worth pointing out that the approximate PDF of Z_m^λ in (26) can be also utilized to minimize the computational complexity of the BEP analysis. Due to the fact that Z_m^λ is assumed to be $\mathcal{N}(0, \sigma_z^2)$ in (26), $P(\hat{X}_m^\lambda | X_m^\lambda = \bar{X}_m^\lambda, K)$ in (29) becomes

$$P(\hat{X}_m^\lambda | X_m^\lambda = \bar{X}_m^\lambda, K) = \frac{1}{\sqrt{2\pi\sigma_z^2}} \times \int_0^\infty \exp\left(-\frac{(Z_m^\lambda + K)^2}{2\sigma_z^2}\right) dZ_m^\lambda. \tag{34}$$

Let $Q(x) = \frac{1}{\sqrt{2\pi}} \int_x^\infty e^{-\frac{-t^2}{2}} dt$ be the Q-function, (34) can be written in terms of the function as

$$P(\hat{X}_m^\lambda | X_m^\lambda = \bar{X}_m^\lambda, K) = Q\left(\frac{K}{\sigma_z}\right). \tag{35}$$

Using $P(\hat{X}_m^\lambda | X_m^\lambda = K)$ from (35) in (32) and (33), the P_e of the systems using BPSK, QPSK and 16-QAM modulation becomes

$$P_e^{\text{BPSK,QPSK}} \simeq Q\left(\frac{1}{\sigma_z}\right), \tag{36a}$$

$$P_e^{\text{16-QAM}} \simeq \frac{3}{4} Q\left(\frac{1}{\sigma_z}\right). \tag{36b}$$

It is evident that the computation complexity of the approximate BEP equations in (36) is much lower complex than that of the accurate BEP analysis in (32) and (33). However, we have found experimentally that these approximate equations provide an accurate BEP if $N_r \geq 10N_t$ and $N_r \geq 100$.

VII. DERIVING PDF OF SNR OF ZF DETECTION

In this section, the effective noise PDFs are used to derive the PDF of the output SNR of ZF detection. If a square-shaped, Gray-coded, M-QAM is selected as modulation scheme, the detector uses the in-phase and quadrature components of the received symbols $\hat{X}_m$ to estimate their information messages independently. In addition, the average symbol energy per dimension for X_m^λ is $E_s/2$ and the output SNR per symbol, γ_s, of their in-phase and quadrature components can be expressed as

$$\gamma_s = \frac{E_s}{2(Z_m^\lambda)^2}. \tag{37}$$

Due to the fact that γ_s in (37) is a function of Z_m^λ, we use (4.19) in [31] to analyze the PDF of γ_s in terms of $p_z(Z_m^\lambda)$, i.e.,

$$p_\gamma(\gamma_s) = \sqrt{\frac{E_s}{2\gamma_s^3}} p_z\left(\sqrt{\frac{E_s}{2\gamma_s}}\right). \tag{38}$$

If the PDF of Z_m^λ in (21) is substituted in (38), $p_\gamma(\gamma_s)$ becomes (39), as shown at the bottom of the next page. In addition, if the approximate PDF of Z_m^λ in (26) is utilized instead of their accurate equation, the PDF of the output SNR of ZF

$$P(\hat{X}_m^\lambda | X_m^\lambda = \bar{X}_m^\lambda, K) = e^{\left(-\frac{2N_r\sigma_h K}{\sigma_w}\right)} \sum_{k=1}^{N_r} \sum_{p=1}^{N_t-1} f_z(k,p) \sum_{q=0}^{N_t-p-1} \frac{1}{(N_t-p-q-1)!q!} \times \left(\frac{(-1)^q (N_t+N_r-k-p)!}{N_r-k+q+1} \sum_{s=0}^{N_t+N_r-k-p} \frac{K^s}{s!} \left(\frac{\sigma_w}{2N_r\sigma_h}\right)^{N_t+N_r-k-p-s+1} + (N_t+N_r-k-p-q-1)!q! \sum_{s=0}^{q} \frac{K^s}{2^{2N_t+2N_r-2k-2p-q-s+1} s!} \left(\frac{\sigma_w}{N_r\sigma_h}\right)^{N_t+N_r-k-p-s+1} + \sum_{r=0}^{N_t+N_r-k-p-q-1} \sum_{s=0}^{N_t+N_r-k-p-r-1} \frac{(-1)^q K^s (N_t+N_r-k-p-q-1)!}{2^{N_t+N_r-k-p+r-s+2}(N_t+N_r-k-p-q-r-1)!s!} \times (N_t+N_r-k-p-r-1)! \left(\frac{\sigma_w}{N_r\sigma_h}\right)^{N_t+N_r-k-p-s+1} \right). \tag{31}$$

detection can be approximated as

$$p_\gamma(\gamma_s) \simeq \sqrt{\frac{E_s}{4\pi\sigma_z^2\gamma_s^3}} \exp\left(-\frac{E_s}{4\gamma_s\sigma_z^2}\right). \quad (40)$$

VIII. OUTAGE PROBABILITY

In this section, the outage probability as a function of the output SNR of the proposed OFDM-M-MIMO system is analyzed utilizing the PDF of γ_s in (39) and the approximate PDF in (40). In general, the outage probability is defined as the probability that γ_s is below a threshold γ_{th}, and this parameter can be evaluated from $p_\gamma(\gamma_s)$ as

$$P_{\text{out}} = \int_0^{\gamma_{th}} p_\gamma(\gamma_s) d\gamma_s. \quad (41)$$

If $p_\gamma(\gamma_s)$ in (39) is substituted in (41), this equation becomes (42), as shown at the bottom of the page. After using (3.351.2) in [33] and the substitution method in [34] to solve the integral operation in this equation, P_{out} of the OFDM-M-MIMO system can be written as (43), as shown at the bottom of the next page. In addition, if the approximate equation in (40) is used by (41), this equation can be expressed as

$$P_{\text{out}} \simeq \sqrt{\frac{E_s}{4\pi\sigma_z^2}} \int_0^{\gamma_{th}} \frac{1}{\sqrt{\gamma_s^3}} \exp\left(-\frac{E_s}{4\gamma_s\sigma_z^2}\right) d\gamma_s. \quad (44)$$

By using the substitution method in [34] to solve the integral operation in (44), P_{out} becomes

$$P_{\text{out}} \simeq \Gamma\left(\frac{E_s}{4\sigma_z^2\gamma_{th}}, 1/2\right). \quad (45)$$

IX. LOW-COMPLEXITY SOFT-OUTPUT ZF DETECTION USING THE DERIVED NOISE VARIANCE

Channel coding is an efficient technique to reduce the BEP in data communications. If the technique is employed by the OFDM-M-MIMO system, the receiver requires soft-output ZF detection to produce the LLRs for channel decoder. Since the exact noise variance of Z_m^λ is required by the detector for producing the LLRs and the computational complexity of the operation significantly increases according to the number of antennas, the detector uses an increased number of the arithmetic operation to evaluate the noise variance. Therefore,

$$\begin{aligned} p_\gamma(\gamma_s) = {} & e^{\left(-\frac{N_r\sigma_h}{\sigma_w}\sqrt{\frac{2E_s}{\gamma_s}}\right)} \sum_{k=1}^{N_r}\sum_{p=1}^{N_t-1} f_z(k,p) \sum_{q=0}^{N_t-p-1} \frac{1}{(N_t-p-q-1)!q!} \\ & \times \left(\frac{(-1)^q}{N_r-k+q+1} \left(\frac{E_s^{N_t+N_r-k-p+1}}{2^{N_t+N_r-k-p+1}\gamma_s^{N_t+N_r-k-p+3}}\right)^{1/2} \right. \\ & + (N_t+N_r-k-p-q-1)! \left(\frac{E_s^{q+1}}{2^{q+1}\gamma_s^{q+3}}\right)^{1/2} \left(\frac{\sigma_w}{4N_r\sigma_h}\right)^{N_t+N_r-k-p-q} \\ & + \sum_{r=0}^{N_t+N_r-k-p-q-1} \frac{(-1)^q(N_t+N_r-k-p-q-1)!}{(N_t+N_r-k-p-q-r-1)!} \left(\frac{E_s^{N_t+N_r-k-p-r}}{2^{N_t+N_r-k-p-r}\gamma_s^{N_t+N_r-k-p-r+2}}\right)^{1/2} \\ & \left. \times \left(\frac{\sigma_w}{4N_r\sigma_h}\right)^{r+1} \right). \end{aligned} \quad (39)$$

$$\begin{aligned} P_{\text{out}} = {} & \sum_{k=1}^{N_r}\sum_{p=1}^{N_t-1} f_z(k,p) \sum_{q=0}^{N_t-p-1} \frac{1}{(N_t-p-q-1)!q!} \\ & \times \left(\frac{(-1)^q}{(N_r-k+q+1)} \left(\frac{E_s}{2}\right)^{(N_t+N_r-k-p+1)/2} \int_0^{\gamma_{th}} \frac{e^{\left(-\frac{N_r\sigma_h}{\sigma_w}\sqrt{\frac{2E_s}{\gamma_s}}\right)}}{\gamma_s^{(N_t+N_r-k-p+3)/2}} d\gamma_s \right. \\ & + (N_t+N_r-k-p-q-1)! \left(\frac{E_s}{2}\right)^{(q+1)/2} \left(\frac{\sigma_w}{4N_r\sigma_h}\right)^{N_t+N_r-k-p-q} \int_0^{\gamma_{th}} \frac{e^{\left(-\frac{N_r\sigma_h}{\sigma_w}\sqrt{\frac{2E_s}{\gamma_s}}\right)}}{\gamma_s^{(q+3)/2}} d\gamma_s \\ & + \sum_{r=0}^{N_t+N_r-k-p-q-1} \frac{(-1)^q(N_t+N_r-k-p-q-1)!}{(N_t+N_r-k-p-q-r-1)!} \left(\frac{E_s}{2}\right)^{(N_t+N_r-k-p-r)/2} \left(\frac{\sigma_w}{4N_r\sigma_h}\right)^{r+1} \\ & \left. \times \int_0^{\gamma_{th}} \frac{e^{\left(-\frac{N_r\sigma_h}{\sigma_w}\sqrt{\frac{2E_s}{\gamma_s}}\right)}}{\gamma_s^{(N_t+N_r-k-p-r+2)/2}} d\gamma_s \right). \end{aligned} \quad (42)$$

we now utilize the derived noise variance in (27) to reduce the computational complexity of the detection. The model of the coded-OFDM-M-MIMO system and the operation of classical soft-output ZF detection are summarized in this section. We then describe the operation of soft-output ZF detector, where the derived noise variance is used. Although several low-complexity soft-output linear symbol detections have been proposed for the M-MIMO system using approximate inverse matrix operation and iterative methods in [3], [4], [5], [6], [7], [8] and [9], most of the works focus on MMSE detection. Since we utilize NSE in [3] to derive the effective noise PDF, we compare the bit error rate (BER) and the computational complexity of the proposed detection with that of the classical soft-output ZF detection, where NSE in the work is employed to reduce the calculation of the LLRs and the noise variance.

Most of the operation of the coded-OFDM-M-MIMO system is identical to that of the conventional uncoded OFDM-M-MIMO, described in the section II. However, the transmitter separates the information bits into N_t sub-streams, and the code words $\mathbf{c}_m \in \mathbb{N}^{1\times N_{\text{coded}}}$ for the m-th transmitter are then generated from the information using the m-th channel encoder, where $\mathbb{N} = \{0, 1\}$ denotes the binary set. The code words are then interleaved and grouped into $\log_2(M)$-tuples. The information is mapped into a M-QAM constellation using the M-QAM mapper, and becomes the M-ary coded symbols. Finally, the IFFT operation produces the OFDM transmit symbol Ψ. If a channel coding technique with the coding rate R is chosen by the coded-OFDM-M-MIMO system, the size of the code words for the m-th transmitter is larger than the number of the information bits, i.e., $N_{\text{coded}} = N_b N_f / R$. Therefore, the variance of W_n for this case is now redefined as

$$\sigma^2_{w,\text{coded}} = \frac{N_t E_s}{2\log_2(M) R \gamma_b}. \tag{46}$$

In addition, after removing the CP, the receiver of the coded-OFDM-M-MIMO system uses the FFT operation to estimate the received symbol in the frequency domain $\mathbf{Y}_f$, and the soft-output ZF detection is then utilized to produce the LLR vector, Λ_f.

We now summarize the operation of the classical low-complexity soft-output ZF detection where NSE in [3] is employed to minimize the computational complexity. The detector uses (3) to estimate $\hat{\mathbf{X}}_f$ from $\mathbf{Y}_f$. Since the computational complexity in the equation is significantly increase according to the number of antennas, the L-th order NSE in (5) is employed to approximate $\mathbf{G}_f^{-1}$ in the equation [3]. Generally, the distribution of Z_m for the m-th antenna is assumed to be the $\mathcal{CN}(0, 2\sigma^2_{z,m})$. If BPSK, QPSK, or M-QAM modulation is chosen by the transmitter, the q-th tuple of the LLR for the m-th antenna is then estimated from the in-phase or the quadrature components of $\hat{X}_m$ as [7]

$$\Lambda_{m,q} = \frac{\min\limits_{\bar{X}_k^\lambda, d_{m,q}=0} (\hat{X}_m^\lambda - \bar{X}_k^\lambda)^2 - \min\limits_{\bar{X}_k^\lambda, d_{m,q}=1} (\hat{X}_m^\lambda - \bar{X}_k^\lambda)^2}{2\sigma^2_{z,m}}. \tag{47}$$

$\sigma^2_{z,m}$ and $\bar{X}_k^\lambda$ in (47) represents the exact noise variance for the m-th transmitter and the constellation points per dimension, respectively. $d_{m,q}$ denotes the q-th tuple of the information bits from the m-th transmitted symbol. Let $\mathbf{U}_{\text{ZF},f} = \mathbf{G}_f^{-1}\mathbf{H}_f^\dagger$ denotes the weight matrix of ZF detection, $\mathbf{Z}_f$ in (4) can be rewritten as $\mathbf{U}_{\text{ZF},f}\mathbf{W}_f$. Therefore, the classical soft-output ZF detection estimates $\sigma^2_{z,m}$ for the m-th transmitter as

$$\sigma^2_{z,m} = \sigma^2_w \sum_{n=1}^{N_r} |U_{n,m}|^2, \tag{48}$$

where an element in $\mathbf{U}_{\text{ZF},f}$ is denoted as $U_{n,m}$. (48) involves an inversion operation of the Gram matrix, resulting in high-complexity. Therefore, the 1-st order NSE is employed to approximate $\mathbf{U}_{\text{ZF},f}$ in the equation as $\mathbf{D}_f^{-1}\mathbf{H}_f^\dagger$ [3]. As a result, the variance in (48) becomes

$$\sigma^2_{z,m} = \frac{\sigma^2_w}{D^2_{m,m}} \sum_{n=1}^{N_r} |H^*_{m,n}|^2. \tag{49}$$

$$\begin{aligned} P_{\text{out}} = {} & e^{\left(-\frac{N_r\sigma_h}{\sigma_w}\sqrt{\frac{2E_s}{\gamma_{th}}}\right)} \sum_{k=1}^{N_r}\sum_{p=1}^{N_t-1} f_z(k,p) \sum_{q=0}^{N_t-p-1} \frac{1}{(N_t-p-q-1)!q!} \\ & \times \left(\frac{(-1)^q (N_t+N_r-k-p)!}{N_r-k+q+1} \left(\frac{E_s^{N_t+N_r-k-p+1}}{2^{N_t+N_r-k-p-1}}\right)^{1/2} \sum_{r=0}^{N_t+N_r-k-p} \frac{1}{r!\sqrt{\gamma_{th}^r}} \left(\frac{\sigma_w}{N_r\sigma_h\sqrt{2E_s}}\right)^{N_t+N_r-k-p-r+1} \right. \\ & + q!(N_t+N_r-k-p-q-1)! \left(\frac{E_s^{q+1}}{2^{q-1}}\right)^{1/2} \left(\frac{\sigma_w}{4N_r\sigma_h}\right)^{N_t+N_r-k-p-q} \sum_{r=0}^{q} \frac{1}{r!\sqrt{\gamma_{th}^r}} \left(\frac{\sigma_w}{N_r\sigma_h\sqrt{2E_s}}\right)^{q-r+1} \\ & + \sum_{r=0}^{N_t+N_r-k-p-q-1} \left(\frac{\sigma_w}{4N_r\sigma_h}\right)^{r+1} \frac{(-1)^q (N_t+N_r-k-p-q-1)!(N_t+N_r-k-p-r-1)!}{(N_t+N_r-k-p-q-r-1)!} \\ & \left. \times \left(\frac{E_s^{N_t+N_r-k-p-r}}{2^{N_t+N_r-k-p-r-2}}\right)^{1/2} \sum_{s=0}^{N_t+N_r-k-p-r-1} \frac{1}{s!\sqrt{\gamma_{th}^s}} \left(\frac{\sigma_w}{N_r\sigma_h\sqrt{2E_s}}\right)^{N_t+N_r-k-p-r-s} \right) \end{aligned} \tag{43}$$

Although (49) requires less arithmetic operations than that of the exact equation in (48) for producing $\sigma^2_{z,m}$, the computational complexity of the equation is still high since the size of $\mathbf{H}_f$ is very large. Moreover, the equation employs the 1-st order NSE to approximate the inverse matrix operation, resulting in a deviation between the outcome from (49) and the exact value of $\sigma^2_{z,m}$. Therefore, a higher accuracy and lower complexity equation for estimating the noise variance is still required for enhancing the BER performance. In section V, we have proved that the PDF of Z^{λ}_m exhibits a normal distribution, i.e., $\mathcal{N}(0, \sigma^2_z)$, and the noise variance can be evaluated using (27). The equation to produce the derived noise variance uses a few arithmetic operators to evaluate the outcome. Therefore, we now use the derived σ^2_z from the equation to produce the LLRs in (47) instead of the approximate noise variance from (49). Empirically, if $N_r \geq 100$ and $N_r/N_t \geq 10$, the derived equation produces an accurate σ^2_z, compared to the exact noise variance. Therefore, the BEP of the coded-OFDM-M-MIMO system, utilizing the derived noise variance is significantly close to that of the general detection for this case.

X. NUMERICAL RESULTS

This research work uses Monte-Carlo simulation to evaluate the analytical results from the proposed equations. The derived effective noise PDFs, the PDF of output SNR, the BEP, and the outage probabilities from the proposed equations are compared with those of the numerical simulations. The OFDM-M-MIMO system and channel model utilized are as described in section II. Gray-coded, QPSK and M-QAM are chosen as modulations schemes for the presented numerical results.

Fig. 2 compares the PDF of the in-phase component of the effective noise Z^I_m from the simulation results with that of the accurate noise PDF in (21) and the Gaussian approximation in (26). 16-QAM was selected for these results, with $N_t = 10$ and $N_r = \{50, 100, 200\}$. A closer look at the graph reveals a good match between analytical and numerical results. For the 10×200 system and $Z^I_m = -2.086$, $p_z(Z^I_m)$ from the accurate noise PDF and simulation result was 3.54×10^{-3} and 3.69×10^{-3}, respectively exhibiting a difference of 1.51×10^{-4}. In addition, the accuracy of the Gaussian approximation PDF was slightly lower than the accurate noise PDF, and the deviation between this equation and simulation results was 1.66×10^{-4}. We also used a 2-sample Kolmogorov–Smirnov test with significance level of 5% to compare the analytical results with that of the empirical. The results confirmed that there is no difference between the outcome from the derived PDFs and the simulation. However, there were small deviations between simulation and analytical results, especially for the system with $N_r = 50$. This is due to the fact that we used $\Delta = 50$ to approximate the value of $D_{m,m}$ in (7), although its true value was ranging between 41 and 59 for 79.93% of the time. Therefore, the maximal deviation between the value of Δ and $D_{m,m}$ was $\pm 18\%$ of its average value, and the outcome from the approximate equation in (9) is inaccurate for this case.

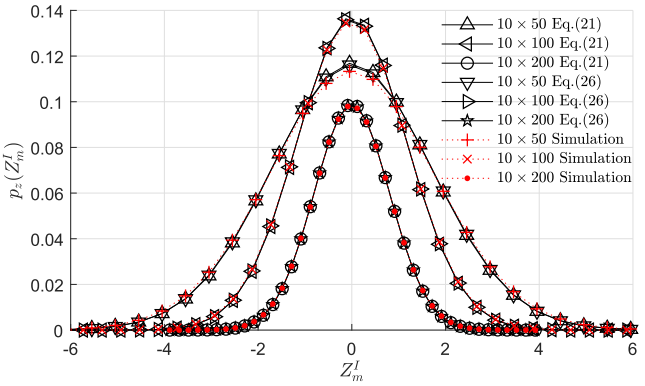

FIGURE 2. The enhanced noise PDF of ZF detection.

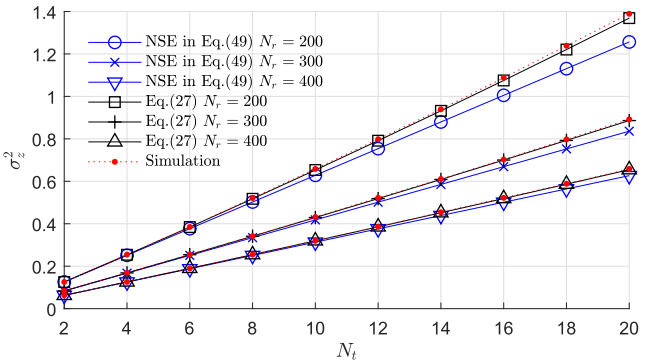

FIGURE 3. Derived effective noise variance for the OFDM-M-MIMO system.

In addition, we employ the derived noise variance in (27) to evaluate the effective noise variance of the OFDM-M-MIMO system in Fig. 3. The outcome of the approximation using NSE in (49) is also included in the figure. The results are also compared to that of the empirical. The system operated at $E_b/N_0 = -10$ dB and the transmitter used the 16-QAM to produce the transmit symbols. $N_r = \{200, 300, 400\}$, and N_t was varied from 2 to 20. The σ^2_z for the OFDM-M-MIMO system, where $N_t > 20$, was not included in the results since the outcome from (27) is inaccurate if the ratio of N_r to N_t is less than 10. According to the results, the outcome from the derived equation was more accurate than that of the NSE. The difference in σ^2_z between the simulation results and the derived equation for the 20×200 OFDM-M-MIMO system was 2.04×10^{-2}. Therefore, the σ^2_z from the proposed equation was only 1.47% different from the simulation result, and the number was 0.11 closer to the exact value than that of the NSE. In addition to the results in Fig. 3, the distribution of the derived noise variance dramatically increases according to N_t. The σ^2_z of the 20×200 OFDM-M-MIMO system was 1.24 higher than that of the 2×200 system. Furthermore, the system using a higher N_r obtained a lower σ^2_z, and the number for the 20×400 system was 0.71 lower than that of the 20×200 system. These results confirm that the OFDM-M-MIMO system using a higher N_r can be efficiently used to reduce the distribution of the effective noise in the detection.

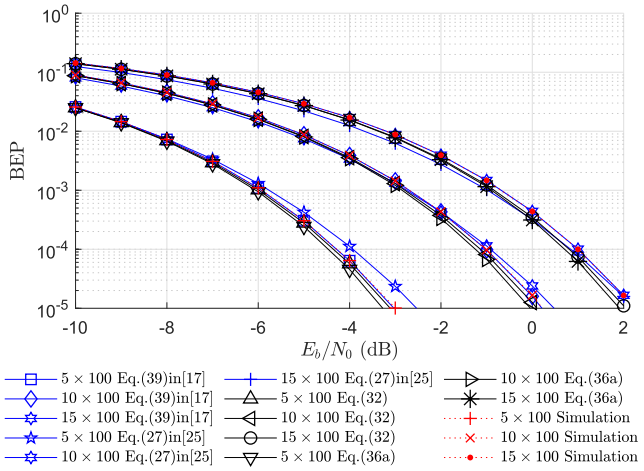

FIGURE 4. BEP of OFDM-M-MIMO system utilizing QPSK modulation.

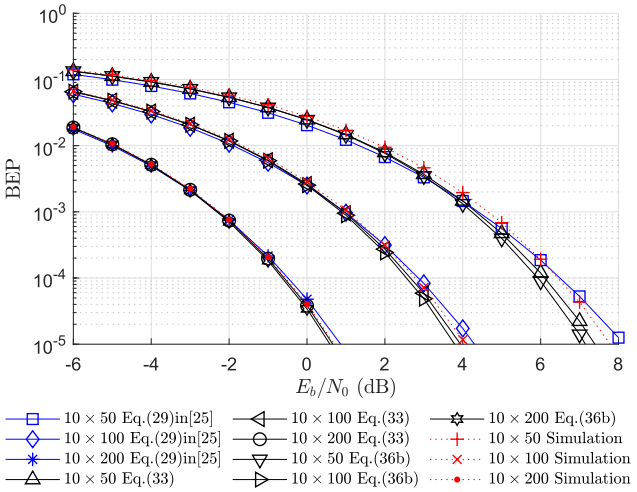

FIGURE 5. BEP of OFDM-M-MIMO system with Gray-coded, 16-QAM.

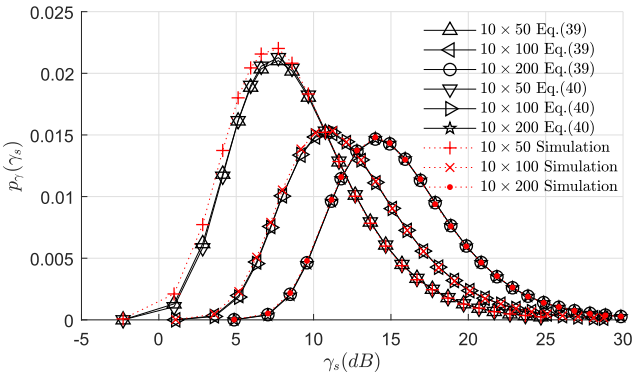

FIGURE 6. Deriving PDF of output SNR for OFDM-M-MIMO system.

The BEP of the OFDM-M-MIMO system using BPSK/QPSK modulation is illustrated in Fig. 4. The analytical results from (32) and those obtained using the approximate equation in (36a) are compared with simulation results. The BEP analysis for QPSK modulation (Eq. (27) in [25]) and BPSK modulation (Eq. (39) in [17]) are also included in the results. We considered the following M-MIMO Tx/Rx antenna combinations, i.e., $N_t = \{3, 6, 9\}$ and $N_r = 100$. Focusing on the 5×100 system, the BEP at $E_b/N_0 = -7$ dB from the exact equation, the approximate equation and the simulation result was 2.93×10^{-3}, 2.8×10^{-3} and 3.08×10^{-3}, respectively. The deviation between the simulation result and the exact equation was only 1.53×10^{-4}. These results confirm that the proposed equations produced an accurate BEP for the OFDM-M-MIMO system. In addition, the BEP analysis of [17], [25] at $E_b/N_0 = -7$ dB was 3.09×10^{-3} and 3.36×10^{-3}, respectively. Therefore, the BEP analysis in (32) was significantly more accurate than the number in [25]. However, the deviation in BEP between the analytical result from the proposed equation and the exact BEP was still higher than that of the BEP in [17] at 1.63×10^{-4}.

Fig. 5 compares the BEP analysis for the OFDM-M-MIMO system using 16-QAM with Gray-encoding from (33) and (36b) with that of simulation results and (29) in [25]. N_t was 10 and $N_r = \{50, 100, 200\}$. Since the equation in [17] was only derived for BPSK modulation, the outcome from the work was not included in the results. According to the results, the proposed equations improved the BEP analysis, and the analytical results for the system with large N_r were closer to the simulation results than that of [25]. In a 10×200 system operating at $E_b/N_0 = 0$ dB, the BEP analysis from the exact equation and the approximate equation were 3.83×10^{-5} and 3.42×10^{-5}, respectively, demonstrating a difference of 2.04×10^{-6} and 6.12×10^{-6} from the simulation results. The number from (29) in [25] was 4.78×10^{-5} and the difference between the analytical and empirical results was 7.53×10^{-6}. Therefore, BEP from the proposed equations was more accurate than that of the equation derived in [25]. However, the results also show that the proposed BEP analysis accuracy is reduced if $N_r/N_t < 10$. Focusing on a 10×50 system operating at $E_b/N_0 = 6$ dB, the difference in BEP between the empirical results and that of (33) was 7.29×10^{-5}, while the value obtained in [25] was only 5.72×10^{-5}.

The PDF of the output SNR using the analytical results in (39) and the approximate results in (40) is shown in Fig. 6. 16-QAM was employed as a modulation scheme operating at an $E_b/N_0 = 0$ dB, with $N_t = 10$ and $N_r = \{50, 100, 200\}$. According to the results, the PDFs from the derived equations matched the simulation results. For a 10×200 system, the value of $p_\gamma(\gamma_s)$ at $\gamma_s = 16$ dB from the simulation was 1.29×10^{-2}, and the difference from the analytical result using (39) was 2.98×10^{-5}. In addition, the PDF from the approximate equation was, as expected, slightly less accurate than the exact equation, i.e., the difference between the result from this equation and the simulation results was 6.22×10^{-5}. The PDFs from the derived equations were also compared using a 2-sample Kolmogorov–Smirnov test with a significance level of 5%, and the results confirm that there is no significant different between simulation and analytical results. However, there was a small deviation between simulation and analytical results for the system with small N_r due to the underlying assumptions made in the derivations.

The effects of N_r in the accuracy of outage probabilities from the derived equations in (43) and (45) are evaluated in

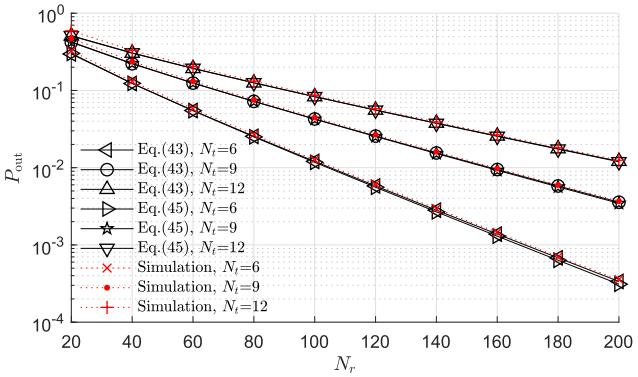

FIGURE 7. The effects of N_r in analytical results for outage probability.

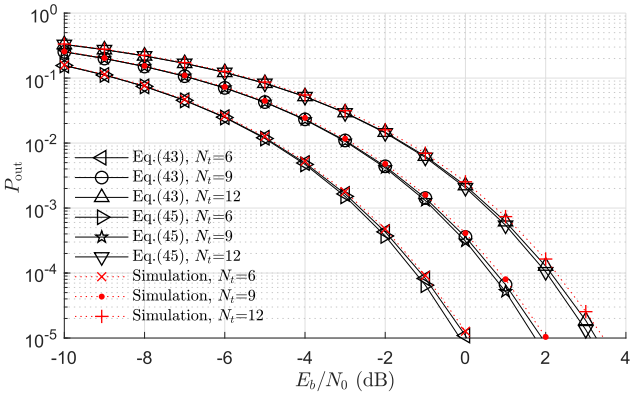

FIGURE 8. Analytical results of outage probability for OFDM-M-MIMO system.

Fig. 7. 16-QAM using Gray encoding operating at $E_b/N_0 = -5$ dB and $\gamma_{th} = -5$ dB. We considered different Tx/Rx antenna combinations, i.e., $N_t = \{6, 9, 12\}$ and N_r varies from 20 to 200 in steps of 20. According to the findings, both equations produced accurate results. For instance, in a 6×200 system, the P_{out} from the simulation result was 3.57×10^{-4}. The numerical values from the derived and approximate equations were 3.37×10^{-4} and 3.1×10^{-4}, respectively, matching very closely to the simulation results. However, there was a small difference between the analytical and simulation results, especially if $N_r < 40$, since the approximation of the value of $D_{m,m}$ utilizing the constant Δ was imprecise.

In addition, Fig. 8 shows the outage probabilities of the system using 16-QAM with Gray encoding. N_r and γ_{th} were 100 and 5 dB, respectively. N_t was 6, 9 and 12. The results confirm that the analytical results from the proposed equations closely matched the simulation results. For the system with $N_t = 6$ and operating at $E_b/N_0 = -1$ dB, the value of P_{out} from the accurate equation was 8.26×10^{-5}, which was only 9.12×10^{-6} away from the simulation result. The deviation between the analytical result from the approximate equation and the simulation was 2.66×10^{-5}, which was slightly higher than that of the accurate equation. However, there were small deviations between the analytical and the simulation results, especially for the system with $N_t = 12$. These differences are due to using the 2-nd order NSE to approximate the inverse matrix operation and analyze the noise PDFs. Empirically, we found that the outcome from the approximate equation is inaccurate if $N_r/N_t < 10$. The deviation between the exact and the derived P_{out} is still high since this condition is not satisfied.

Fig. 9 shows the BER of coded-OFDM-M-MIMO system where the low-complexity soft-output ZF detection, and the derived noise variance in (27) are utilized by the receiver for producing the LLR in (47). The detector employed the 3-rd order NSE to simplify the operation in (3) for producing $\hat{\mathbf{X}}_f$ from $\mathbf{Y}_f$. We compare the BER with that of the system using the approximate $\sigma^2_{z,m}$ in (49). In addition, the BER of the classical soft-output detector, using general inverse matrix operation and the exact noise variance in (48), is also included in the results. The block size utilization was 1024 bits and 16-QAM was chosen by the system. We used an uplink 5G NR LDPC with the base matrix 1 and the revision number 0 to encode the information bits. The channel decoder used the Belief propagation to estimate the transmitted information from the LLR. The coding rate and the number of iteration were 1/2 and 25, respectively. N_t was 10 and $N_r = \{50, 100, 200\}$. A pseudo-random interleaver was chosen for the simulation for converting burst errors to random error events. Evidently, the difference in BER between the system using the proposed detection and that of the classical detection was small, especially for a system with a higher N_r. The 10×50 system using the proposed detection required $E_b/N_0 = -1.8$ dB to maintain the BER of 10^{-3}, which was 0.47 dB higher than that of the classical detection. If $N_r = 200$, the difference in E_b/N_0 between the system using the derived noise variance and the classical detection at BER of 10^{-3} was smaller at 1.35×10^{-2} dB. Furthermore, the BER for the system using the derived noise variance was less than that of the approximate noise variance. Focusing on the 10×50 system at $E_b/N_0 = -2$ dB, the BER of the proposed system was 3.15×10^{-3}, which was 2.79×10^{-3} lower than that of the system with the approximate noise variance.

In addition to the soft-output ZF detection, Table 1 demonstrates the number of real arithmetic operators, which are required for producing the LLRs for all N_f sub-carriers in (47). The proposed soft-output ZF detection utilized (27) to evaluate the noise variance for producing the LLR, whereas the general detection employed the approximate noise variance in (49) for the operation. Total complex operations, which was required to determine the LLR from $\hat{X}^{\lambda}_m$, were determined in terms of real arithmetic operations. We assumed that the operation to evaluate the minimal value of X variables requires $X-1$ comparisons, and the summation of X variables uses $X - 1$ additions. Since the derived noise variance was a function of constants, the variable was evaluated only one time for all sub-carriers. In addition, the number of arithmetic operations, required for producing $\mathbf{D}_f$ in (49), was not included in the results since the diagonal components of the Gram matrix were previously generated by (3) for producing $\hat{X}^{\lambda}_m$. Although the number of comparisons in both detections was equal, the proposed detection required less

TABLE 1. Comparison of real-arithmetic operations in soft-output ZF detection.

Number of real arithmetic operators	ZF detection using NSE and approximate noise variance in (49)	Proposed ZF detection using NSE and derived noise variance in (27)
Addition and subtraction	$N_t N_f(\log_2(M)+2M_\lambda+2N_r-1)$	$N_t N_f(\log_2(M)+2M_\lambda)+2$
Multiplication	$N_t N_f(2M_\lambda+2N_r+3)$	$N_t N_f(2M_\lambda+1)+3$
Division	$N_t N_f(\log_2(M)+1)$	$N_t N_f \log_2(M)+3$
Comparison	$N_t N_f \log_2(M)(M_\lambda-2)$	$N_t N_f \log_2(M)(M_\lambda-2)$

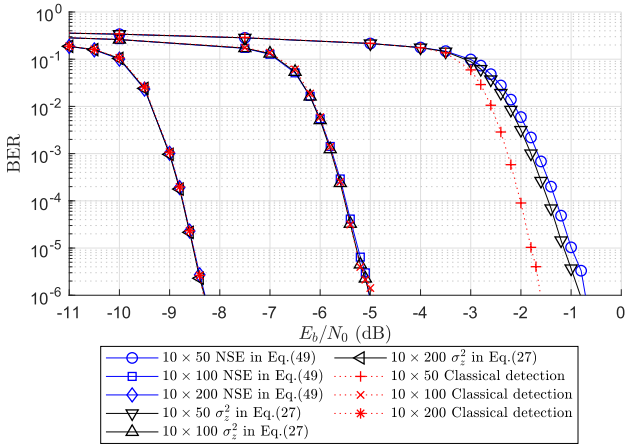

FIGURE 9. BER of coded-OFDM-M-MIMO system using low-complexity soft-output ZF detection.

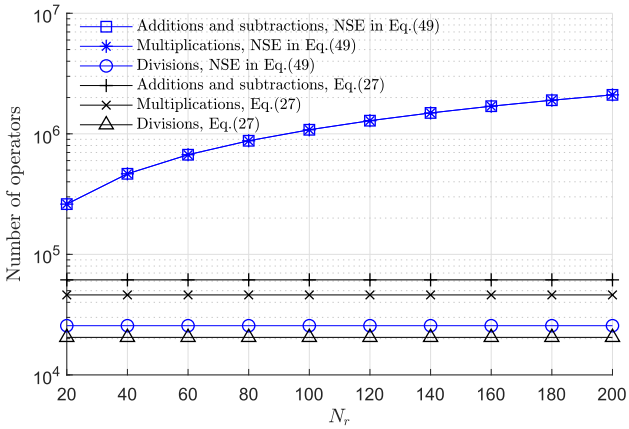

FIGURE 10. Computational complexity of soft-output ZF detection.

additions, subtractions, multiplications, and divisions than that of the general detection. Fig. 10 shows the number of real arithmetic operators, required for the detections in the OFDM-M-MIMO system, using 16-QAM, $N_t = 10$ and $N_f = 512$ symbols. The size of N_r was varied from 20 to 200. Evidently, utilizing the derived noise variance provided a massive reduction in real arithmetic operators to the ZF detector. If $N_r = 200$, the number of additions and subtractions for the classical and the proposed detection was 2.1×10^6 and 6.14×10^4, respectively. Therefore, 97.08% of the arithmetic operations can be reduced by utilizing the derived noise variance. In addition, the number of multiplications significantly reduced from 2.1×10^6 to 4.61×10^4. The results demonstrated that 97.81% of multiplications in the soft-output ZF detection can be minimized by utilizing the proposed detection.

XI. CONCLUSION

In this paper, an accurate PDF is derived using the effective noise in a OFDM-M-MIMO system, where ZF detection is used along with Gray-coded BPSK, QPSK, and M-QAM modulation. We use joint probabilities of random variables involved in the system model to derive their PDFs. Since the computational complexity of the accurate PDFs derived was too high, the Gaussian approximation of the effective noise PDF was additionally derived. The obtained PDFs were subsequently utilized to compute the BEP performance, the PDF of the output SNR, and the outage probability of the proposed OFDM-M-MIMO system. The simulations confirmed that the outcomes from the derived equations were closely matching the numerical results. Although the computational complexity of the approximation is minimized, the deviation between the analytical result from the approximate equations and the exact results was small, especially if $N_r \geq 100$. Therefore, they can be efficiently used to evaluate performance of OFDM-M-MIMO system. In addition, we employed the derived noise variance to produce the LLRs utilized in soft-output ZF detection. By utilizing the proposed detection, the number of arithmetic operators, required for producing the LLRs, can be significantly decreased. There is a very small reduction in BER performance compared to the classical detection, and the proposed detection requires less E_b/N_0 to maintain the BER than that of the soft-output detection using NSE. Thus, the proposed soft-output detection can be efficiently utilized for reducing the computational complexity in coded OFDM-M-MIMO systems.

Although the BEP from the proposed exact and the approximate equations is more accurate than that of the BEP in [25], a number of approximations were chosen for this research work. The diagonal components of the Gram matrix are assumed to be a constant and this approximation is precise if $N_r \geq 100$. This work presented closed-form BEP for M-QAM modulations using 2-nd order NSE in (5) and extending the BPSK work in [17] to general M-QAM formats for $N_r > 10N_t$. To overcome the latter limitation, future research work will consider a higher order NSE, the presence of diagonal components in the Gram matrix as well as other types of inverse matrix operations. Furthermore, more accurate channel model for the system using OFDM waveform should be included in the work for improving the performance analysis.

REFERENCES

[1] E. G. Larsson, O. Edfors, F. Tufvesson, and T. L. Marzetta, "Massive MIMO for next generation wireless systems," *IEEE Commun. Mag.*, vol. 52, no. 2, pp. 186–195, Feb. 2014.

[2] S. Yang and L. Hanzo, "Fifty years of MIMO detection: The road to large-scale MIMOs," *IEEE Commun. Surveys Tuts.*, vol. 17, no. 4, pp. 1941–1988, 4th Quart., 2015.

[3] M. Wu, B. Yin, G. Wang, C. Dick, J. R. Cavallaro, and C. Studer, "Large-scale MIMO detection for 3GPP LTE: Algorithms and FPGA implementations," *IEEE J. Sel. Topics Signal Process.*, vol. 8, no. 5, pp. 916–929, Oct. 2014.

[4] C. Xiao, X. Su, J. Zeng, L. Rong, X. Xu, and J. Wang, "Low-complexity soft-output detection for massive MIMO using SCBiCG and Lanczos methods," *China Commun.*, vol. 12, pp. 9–17, Dec. 2015.

[5] L. Dai, X. Gao, X. Su, S. Han, I. Chih-Lin, and Z. Wang, "Low-complexity soft-output signal detection based on Gauss–Seidel method for uplink multiuser large-scale MIMO systems," *IEEE Trans. Veh. Technol.*, vol. 64, no. 10, pp. 4839–4845, Oct. 2015.

[6] X. Qin, Z. Yan, and G. He, "A near-optimal detection scheme based on joint steepest descent and Jacobi method for uplink massive MIMO systems," *IEEE Commun. Lett.*, vol. 20, no. 2, pp. 276–279, Feb. 2016.

[7] M. Zhang and S. Kim, "Evaluation of MMSE-based iterative soft detection schemes for coded massive MIMO system," *IEEE Access*, vol. 7, pp. 10166–10175, 2019.

[8] S. Berra, M. A. M. Albreem, M. Malek, R. Dinis, X. Li, and K. M. Rabie, "A low-complexity soft-output signal data detection algorithm for UL massive MIMO systems," in *Proc. Int. Conf. Comput., Inf. Telecommun. Syst. (CITS)*, Nov. 2021, pp. 1–6.

[9] C. Zhang, Z. Wu, C. Studer, Z. Zhang, and X. You, "Efficient soft-output Gauss–Seidel data detector for massive MIMO systems," *IEEE Trans. Circuits Syst. I, Reg. Papers*, vol. 68, no. 12, pp. 5049–5060, Dec. 2021.

[10] M. A. Albreem, M. Juntti, and S. Shahabuddin, "Massive MIMO detection techniques: A survey," *IEEE Commun. Surveys Tuts.*, vol. 21, no. 4, pp. 3109–3132, 4th Quart., 2019.

[11] J. H. Winters, J. Salz, and R. D. Gitlin, "The capacity of wireless communication systems can be substantially increased by the use of antenna diversity," in *Proc. 1st Int. Conf. Universal Pers. Commun.*, 1992, pp. 02.01/1–02.01/5.

[12] J. H. Winters, J. Salz, and R. D. Gitlin, "The impact of antenna diversity on the capacity of wireless communication systems," *IEEE Trans. Commun.*, vol. 42, no. 234, pp. 1740–1751, Feb./Mar./Apr. 1994.

[13] R. Xu and F. C. M. Lau, "Performance analysis for MIMO systems using zero forcing detector over Rice fading channel," in *Proc. IEEE Int. Symp. Circuits Syst.*, vol. 5, May 2005, pp. 4955–4958.

[14] H. A. Saleh and W. Hamouda, "Performance of zero-forcing detectors over MIMO flat-correlated Ricean fading channels," *IET Commun.*, vol. 3, no. 1, pp. 10–16, Jan. 2009.

[15] D. Gore, R. W. Heath, Jr., and A. Paulraj, "On performance of the zero forcing receiver in presence of transmit correlation," in *Proc. IEEE Int. Symp. Inf. Theory*, Jun./Jul. 2002, p. 159.

[16] H.-Y. Fan, "MIMO detection schemes for wireless communications," MPhil. thesis, Dept. Elect. Electron. Eng., Hong Kong Univ. Sci. Technol., Hong Kong, 2002.

[17] Y. Jiang, M. K. Varanasi, and J. Li, "Performance analysis of ZF and MMSE equalizers for MIMO systems: An in-depth study of the high SNR regime," *IEEE Trans. Inf. Theory*, vol. 57, no. 4, pp. 2008–2026, Apr. 2011.

[18] G. Alfano, C.-F. Chiasserini, and A. Nordio, "SINR and multiuser efficiency gap between MIMO linear receivers," *IEEE Trans. Wireless Commun.*, vol. 19, no. 1, pp. 106–119, Jan. 2020.

[19] C. Siriteanu, Y. Miyanaga, S. D. Blostein, S. Kuriki, and X. Shi, "MIMO zero-forcing detection analysis for correlated and estimated Rician fading," *IEEE Trans. Veh. Technol.*, vol. 61, no. 7, pp. 3087–3099, Sep. 2012.

[20] C. Wang, E. K. S. Au, R. D. Murch, W. H. Mow, R. S. Cheng, and V. Lau, "On the performance of the MIMO zero-forcing receiver in the presence of channel estimation error," *IEEE Trans. Wireless Commun.*, vol. 6, no. 3, pp. 805–810, Mar. 2007.

[21] F. Jiang, C. Li, and Z. Gong, "Accurate analytical BER performance for ZF receivers under imperfect channel in low-SNR region for large receiving antennas," *IEEE Signal Process. Lett.*, vol. 25, no. 8, pp. 1246–1250, Aug. 2018.

[22] C. D. Altamirano, J. Minango, H. C. Mora, and C. De Almeida, "BER evaluation of linear detectors in massive MIMO systems under imperfect channel estimation effects," *IEEE Access*, vol. 7, pp. 174482–174494, 2019.

[23] J. Lu, K. B. Letaief, J. C.-I. Chuang, and M. L. Liou, "M-PSK and M-QAM BER computation using signal-space concepts," *IEEE Trans. Commun.*, vol. 47, no. 2, pp. 181–184, Feb. 1999.

[24] J. G. Proakis, *Digital Communications*, 5th ed. New York, NY, USA: McGraw-Hill, 2008.

[25] A. J. Al-Askery, C. C. Tsimenidis, S. Boussakta, and J. A. Chambers, "Performance analysis of coded massive MIMO-OFDM systems using effective matrix inversion," *IEEE Trans. Commun.*, vol. 65, no. 12, pp. 5244–5256, Dec. 2017.

[26] G. L. Stüber, *Principles of Mobile Communication*, 4th ed. Cham, Switzerland: Springer, 2017.

[27] P. Dharmawansa, N. Rajatheva, and H. Minn, "An exact error probability analysis of OFDM systems with frequency offset," *IEEE Trans. Commun.*, vol. 57, no. 1, pp. 26–31, Jan. 2009.

[28] D. Singh, A. Kumar, H. D. Joshi, M. Magarini, and R. Saxena, "Symbol error rate analysis of OFDM system with CFO over TWDP fading channel," *Wireless Pers. Commun.*, vol. 109, no. 4, pp. 2187–2198, Dec. 2019.

[29] D. Singh and H. D. Joshi, "Performance analysis of SFBC-OFDM system with channel estimation error over generalized fading channels," *Trans. Emerg. Telecommun. Technol.*, vol. 29, no. 3, p. e3293, Mar. 2018.

[30] D. Singh and H. D. Joshi, "Error probability analysis of STBC-OFDM systems with CFO and imperfect CSI over generalized fading channels," *AEU, Int. J. Electron. Commun.*, vol. 98, pp. 156–163, Jan. 2018.

[31] A. Grami, *Probability, Random Variables, Statistics, and Random Processes: Fundamentals and Applications*. Hoboken, NJ, USA: Wiley, 2020.

[32] M. K. Simon, *Probability Distributions Involving Gaussian Random Variables: A Handbook for Engineers and Scientists*. New York, NY, USA: Springer, 2006.

[33] A. Jeffrey and D. Zwillinger, *Table of Integrals, Series, and Products*, 6th ed. New York, NY, USA: Academic, 2000.

[34] G. R. Iversen, *Calculus*. Newbury Park, CA, USA: Sage, 1996.

DITSAPON CHUMCHEWKUL received the B.Eng. degree in electrical and electronics engineering from the King Mongkut's Institute of Technology North Bangkok, in 2000, and the M.Eng. degree in information engineering from the King Mongkut's Institute of Technology Ladkrabang, in 2003. He is currently pursuing the Ph.D. degree in electrical and electronics engineering with the School Engineering, Newcastle University. He is also a Lecturer with the Department of Telecommunication Engineering, Faculty of Engineering, Rajamangala University of Technology Rattanakosin. His education in M.Eng. and Ph.D. degrees was supported by the scholarships from Thailand's National Science and Technology Development Agency, the Thailand Graduate Institute of Science and Technology, the Office of the Civil Service Commission, the Royal Thai Embassy, The Office of Educational Affairs, and the Rajamangala University of Technology Rattanakosin. He has published more than 14 conference papers, a letter, and a journal articles. His research interests include wireless communications, optical wireless communications, and channel coding techniques.

CHARALAMPOS C. TSIMENIDIS (Senior Member, IEEE) received the Ph.D. degree in communications and signal processing from Newcastle University, in 2002. He is currently a Professor of digital innovation at Nottingham Trent University. He has published over 230 conference and journal papers, supervised successfully three M.Phil. and 50 Ph.D. students and made contributions in the area of digital communications to several U.K. and European funded research projects. His main research interests include digital communications and signal processing with specialization in massive multiple-input multiple-output systems, adaptive filter, and demodulation algorithms, error control and network coding for radio frequency, and underwater acoustic channels. He is a member of the IET.